The Simulation of Mixing Layers Driven by Compound Buoyancy and Shear

D. M. Snider
Senior Engineer,
Science Applications
International Corporation,
2109 Air Park, SE,
Albuquerque, NM 87106

M. J. Andrews
Assistant Professor,
Department of Mechanical Engineering,
Texas A&M University,
College Station, TX 77843

Fully developed compound shear and buoyancy driven mixing layers are predicted using a k-ϵ turbulence model. Such mixing layers present an exchange of equilibrium in mixing flows. The k-ϵ buoyancy constant $C_{\epsilon 3}$ = 0.91, defined in this study for buoyancy unstable mixing layers, is based on an approximate self-similar analysis and an accurate numerical solution. One-dimensional transient and two-dimensional steady calculations are presented for buoyancy driven mixing in a uniform flow field. Two-dimensional steady calculations are presented for compound shear and buoyancy driven mixing. The computed results for buoyancy alone and compound shear and buoyancy mixing compare well with measured data. Adding shear to an unstable buoyancy mixing layer does not increase the mixing growth rate compared with that from buoyancy alone. The nonmechanistic k-ϵ model which balances energy generation and dissipation using constants from canonical shear and buoyancy studies predicts the suppression of the compound mixing width. Experimental observations suggest that a reduction in growth rate results from unequal stream velocities that skew and stretch the normally vertical buoyancy plumes producing a reduced mixing envelope width.

Introduction

An unstable thermal stratification occurs when cold fluid overlays warm fluid under the influence of gravity. The buoyancy of the cool (heavy fluid) above the warmer (light fluid) makes the thermal interface unstable and causes the two fluids to mix. More generally, an acceleration directed from the heavy fluid to the light fluid imposes a pressure gradient at the density interface that drives the development of Rayleigh-Taylor instability (Taylor, 1950 and Chandrasekhar, 1961). The initial linear instability gives way to nonlinear mixing as heavy fluid falls through light fluid and light fluid rises through heavy fluid. In the nonlinear, three-dimensional process, vortices form between the moving fluid interfaces which leads to turbulent mixing. More typical of an application is that buoyancy often is accompanied by shear. Buoyancy produces a normal force at the interface, while parallel streams of unequal velocity produce a tangential shear force at the interface. Free shear perturbations arise as Kelvin-Helmholtz instabilities and are followed by growth and pairing of vortices that eventually form a turbulent mixing layer as observed by Brown and Roshko (1974).

Unstable thermal stratification occurs in both environmental and industrial processes (Sharp, 1984). Compound buoyancy and shear mixing occur in nature from effluent discharge into rivers and estuaries or from flow into ponds, lakes, or reservoirs (Imberger and Hamblin, 1982). Above the atmospheric boundary layer, buoyancy turbulence from phase change forms orderly plumes of cumulus clouds (Deardorff, 1970 and Vinnichenko et al., 1980). In heat exchangers, cold fluid enters the top of the exchanger, falls rapidly, and mixes with the warm fluid underneath. Swirl is used in pipes and internal combustion engines to generate an unstable thermal layer and promote heat transfer (Dhir and Chang, 1992). Furnaces and combustion chambers introduce cool fuel mixtures over hot gases, and chemical reactors mix chemicals of different densities. All these applications exhibit closely coupled compound buoyancy and shear flows. This close coupling between canonical shear and buoyancy results in compound interactions that are poorly understood and lead to a novel mixing process. Indeed, this compound buoyancy and shear presents an intriguing situation of two canonical equilibrium flows that exchange equilibria as the flow develops. Developed shear layers grow linearly with distance (Rajaratnam, 1976), while unstable buoyancy driven layers grow quadratically with streamwise distance (Youngs, 1984). The mixing process progresses through shear dominated flow with a linear growth rate to end with buoyancy mixing with a quadratic growth rate.

Calculations for developed shear layers have been made with turbulence models, such as that by Launder et al. (1973), and by direct numerical solution such as that by Comte et al. (1989) and Rogers and Moser (1994). Rayleigh-Taylor mixing from initially stagnant layers has been calculated using a transient, two-fluid model without a turbulence model by Youngs (1991), and a direct numerical solution by Li (1993). The prediction of compound buoyancy and shear mixing has been largely directed at the stable mixing layer (light fluid above heavy fluid). However, Andrews and Spalding (1990) reported "tilted" experiments where large scale overturning motion superimposed a shearing across a Rayleigh-Taylor mixing interface. Snider and Andrews (1994) presented detailed experiments of compound shear and unstable buoyancy mixing.

This study simulates fully developed compound shear and unstable buoyancy mixing in a plane layer using a two-equation turbulence model. Figure 1 illustrates a compound shear and buoyancy mixing layer. Turbulence transport is modeled by an eddy-diffusivity relation with closure completed using a two equation k-ϵ turbulence model. The k-ϵ turbulence closure model (Launder and Spalding, 1974) was chosen because of its popularity and its success in predicting a variety of turbulent flows. The model has recognized limitations (Bradshaw et al., 1991) with one major shortcoming being that its accuracy partly depends on empirical constants tailored for specific situations. This is especially true of the buoyancy dissipation constant $C_{\epsilon 3}$ (Eq. (7)). Reported values for $C_{\epsilon 3}$ range from 0.8 to 1.44 and are often defined together with a Richardson number (Rodi, 1991, 1993 and Yang and Aung, 1985). Launder (1988) used

Contributed by the Fluids Engineering Division for publication in the JOURNAL OF FLUIDS ENGINEERING. Manuscript received by the Fluids Engineering Division September 26, 1994; revised manuscript received September 7, 1995. Associate Technical Editor: S. P. Vanka.

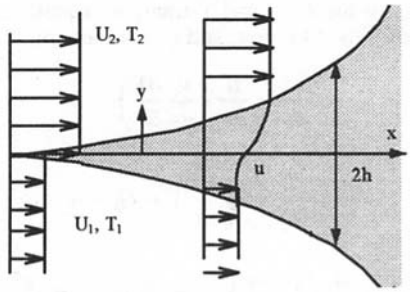

Fig. 1 Illustration of the buoyancy and shear mixing layer

$C_{\epsilon 3} = C_{\epsilon 1}$ in calculating flow near a heated vertical wall. Hanjalic and Vasic (1993) reported $C_{\epsilon 3} = 0.8$ for an accurate prediction of pure buoyancy driven flows. In this study, the turbulence constant $C_{\epsilon 3}$ that appears in the buoyancy term of the dissipation is carefully evaluated from an analytical self-similar solution and an accurate numerical solution.

The turbulence model has been used successfully to simulate stable stratified flows where buoyancy suppresses the growth of the shear layer (Tennekes and Lumley, 1972). Calculations in this study are presented for unstable buoyancy and shear driven mixing. It might be expected that addition of the two unstable mixing mechanisms would increase the mixing layer growth rate beyond that of either of the two individual layers. This study shows that the k-ϵ model predicts a suppression of the buoyancy layer growth rate from addition of shear. The structure of experimentally measured data is examined to evaluate the validity of the calculated behavior. From a practical point this result indicates that shear can be used to mitigate the mixing growth due to unstable buoyancy, or conversely, unstable buoyancy can be used as a limited means to promote shear mixing.

Experimental Data. This numerical work makes use of experimental data from Snider and Andrews (1994) who developed a statistically steady experiment where buoyancy and shear were copresent and independently controlled. Details of the experiment can be found in Snider and Andrews (1994). Two parallel flowing water streams were separated by a thin splitter plate. At the end of the splitter plate, the flows met. A buoyancy unstable interface formed if the stream temperatures were different. An unstable shearing interface formed if the velocities were different, and a compound mixing layer formed if both temperatures and velocities were different. The mixing angle was chosen to be small to ensure parabolic flow.

Governing Equations and k-ϵ Model

The water mixing layer is a Newtonian incompressible fluid with constant kinematic viscosity. Temperature differences are small and density variations are limited to the buoyancy terms using the Boussinesq approximation. The ensemble averaged equations for conservation of mass, momentum, and energy equations are:

$$\frac{\partial u}{\partial x} + \frac{\partial v}{\partial y} = 0 \tag{1}$$

$$\frac{\partial u}{\partial t} + u\frac{\partial u}{\partial x} + v\frac{\partial u}{\partial y} = -\frac{1}{\rho}\frac{\partial p}{\partial x} + \nu\left[\frac{\partial^2 u}{\partial x^2} + \frac{\partial^2 u}{\partial y^2}\right] - \left[\frac{\partial \overline{u'u'}}{\partial x} + \frac{\partial \overline{u'v'}}{\partial y}\right] \tag{2}$$

$$\frac{\partial v}{\partial t} + u\frac{\partial v}{\partial x} + v\frac{\partial v}{\partial y} = -\frac{1}{\rho}\frac{\partial p}{\partial y} + \nu\left[\frac{\partial^2 v}{\partial x^2} + \frac{\partial^2 v}{\partial y^2}\right] - \left[\frac{\partial \overline{v'u'}}{\partial x} + \frac{\partial \overline{\partial v'v'}}{\partial y}\right] + \beta g(T - T_o) \tag{3}$$

$$\frac{\partial T}{\partial t} + u\frac{\partial T}{\partial x} + v\frac{\partial T}{\partial y} = \frac{\kappa}{\rho C_p}\left[\frac{\partial^2 T}{\partial x^2} + \frac{\partial^2 T}{\partial y^2}\right] - \left[\frac{\partial \overline{T'u'}}{\partial x} + \frac{\partial \overline{T'v'}}{\partial y}\right] \tag{4}$$

where u and v are ensemble average velocities and p, ρ, and T are ensemble averaged pressure, density, and temperature, respectively. The expansion coefficient is $\beta = -(1/\rho_o)/(\partial\rho/\partial T)$, and T_o and ρ_o are the mean temperature and corresponding density. The u', v', ρ', and T' are fluctuating components. The $\overline{u'u'}$, $\overline{v'v'}$, and $\overline{u'v'}$ are the ensemble averaged Reynolds stresses, and $\overline{u'T'}$ and $\overline{v'T'}$ are the turbulent heat fluxes. Closure is completed using a Boussinesq approximation and a turbulent kinetic energy and kinetic energy dissipation model. The equations of closure are:

$$\overline{u'u'} = -\nu_t\left(2\frac{\partial u}{\partial x}\right) + \frac{2}{3}k \quad \overline{v'v'} = -\nu_t\left(2\frac{\partial v}{\partial y}\right) + \frac{2}{3}k$$

$$\overline{u'v'} = -\nu_t\left(\frac{\partial u}{\partial y} + \frac{\partial v}{\partial x}\right) \tag{5a}$$

Nomenclature

A = Atwood number: A = $(\rho_1 - \rho_2)/(\rho_1 + \rho_2)$
C_μ, $C_{\epsilon 1}$, $C_{\epsilon 2}$, $C_{\epsilon 3}$ = constants in turbulence model
C_W, C_k, C_ϵ, C_ρ = constants in assumed self-similar profiles
B = equation (20)
g = gravity acceleration
G_s = production of kinetic energy from shear
G_b = production of kinetic energy from buoyancy
h = half-width of the mixing layer (see Fig. 1 and Fig. 8)
k = ensemble averaged turbulent kinetic energy
l = turbulent length scale
p = ensemble averaged pressure
Ri = Richardson number
t = time
T = ensemble averaged temperature
T_0 = reference temperature
T_1, T_2 = freestream temperatures
u, v = ensemble averaged velocities
u', v' = fluctuating velocities
U_1, U_2 = freestream velocities
x, y = spatial coordinate in streamwise and vertical directions, respectively
α = buoyancy growth constant
β = coefficient of expansion
δ_ω = vorticity thickness
κ = thermal conductivity
ν = kinematic viscosity
ν_t = turbulent kinematic viscosity
T' = fluctuating temperature
$\overline{u_i'u_j'}$ = Reynolds stress
$\overline{T'u_j'}$ = fluctuating components of temperature
ϵ = ensemble averaged kinetic energy dissipation
ϵ_T = ensemble averaged turbulence heat flux dissipation
η = buoyancy similarity variable y/t^2
ρ = ensemble averaged density
ρ_1, ρ_2 = freestream densities
ρ_o = reference density at T_o
ρ' = fluctuating density
σ_T, σ_k, σ_ϵ, = Prandtl numbers

where the turbulent viscosity is $\nu_t = C_\mu(k^2/\epsilon)$. The closure for the turbulent heat flux is an eddy diffusivity model with the thermal time scale, $\overline{T'^2}/2\epsilon_T$, equal to the mechanical time scale, k/ϵ where ϵ_T is the molecular diffusion of turbulent temperature variance (Hanjalic, 1994):

$$\overline{T'u'} = -\frac{\nu_t}{\sigma_T}\left(\frac{\partial T}{\partial x}\right) \quad \overline{T'v'} = -\frac{\nu_t}{\sigma_T}\left(\frac{\partial T}{\partial y}\right) \tag{5b}$$

The simple gradient model neglects two important effects. First, the model does not predict an intensive turbulent heat flux where the mean temperature gradient is uniform or where the gradient may be in the same direction as the heat flux vector. Second, at a vertical heated wall where the major source of turbulence is induced by vertical heat flux, the temperature gradient in the vertical direction is small. This study of the unstable buoyancy layer does not suffer from the above two shortcomings. Buoyancy induced turbulence is in the direction of turbulent heat flux and opposite the temperature gradient.

The ensemble averaged turbulent kinetic energy and the dissipation equations are:

$$\frac{\partial k}{\partial t} + u\frac{\partial k}{\partial x} + v\frac{\partial k}{\partial y} = \frac{\partial}{\partial x}\left(\frac{\nu_t}{\sigma_k}\frac{\partial k}{\partial x}\right) + \frac{\partial}{\partial y}\left(\frac{\nu_t}{\sigma_k}\frac{\partial k}{\partial y}\right) + G_s + G_b - \epsilon \tag{6}$$

$$\frac{\partial \epsilon}{\partial t} + u\frac{\partial \epsilon}{\partial x} + v\frac{\partial \epsilon}{\partial y} = \frac{\partial}{\partial x}\left(\frac{\nu_t}{\sigma_\epsilon}\frac{\partial \epsilon}{\partial x}\right) + \frac{\partial}{\partial y}\left(\frac{\nu_t}{\sigma_\epsilon}\frac{\partial \epsilon}{\partial y}\right) + C_{\epsilon 1}\frac{\epsilon}{k}G_s + C_{\epsilon 3}\frac{\epsilon}{k}G_b - C_{\epsilon 2}\frac{\epsilon^2}{k} \tag{7}$$

where k and ϵ are ensemble averaged kinetic energy and kinetic energy dissipation, respectively. The turbulent diffusivity is assumed much larger than the molecular diffusivity. The turbulent kinetic energy production from shear for two-dimensional incompressible flow is:

$$G_s = \nu_t\left[2\left(\frac{\partial u}{\partial x}\right)^2 + 2\left(\frac{\partial v}{\partial y}\right)^2 + \left(\frac{\partial u}{\partial y} + \frac{\partial v}{\partial x}\right)^2\right] \tag{8}$$

and the turbulent kinetic energy production from buoyancy is:

$$G_b = \frac{\nu_t g}{\sigma_T \rho_o}\frac{\partial \rho}{\partial y} = -\frac{\nu_t g}{\sigma_T}\beta\frac{\partial T}{\partial y} \tag{9}$$

where g is gravity, and σ_T is the Prandtl number.

The k-ϵ constants are $C_\mu = 0.09$, $C_{\epsilon 1} = 1.44$, $C_{\epsilon 2} = 1.92$, $\sigma_k = 1$, and $\sigma_\epsilon = 1.3$ (Launder and Spalding, 1974), and $\sigma_T = 0.6$ for the free mixing layer calculations (White, 1991). The constant $C_{\epsilon 3}$ is assigned the value 0.91 in this study.

Determination of $C_{\epsilon 3}$

The $C_{\epsilon 3}$ constant in Eq. (7) for Rayleigh-Taylor mixing in a plane layer is defined here. A value is determined from an approximate analytical self-similar solution and then with an accurate numerical solution.

Self-Similar Buoyancy Mixing. Here we describe a one-dimensional self-similar solution for the present problem similar to that of Andrews (1984) and a later analysis by Spitz and Haas (1991). In the experimental arrangement (Snider and Andrews, 1994) a buoyancy driven turbulent mixing layer grows when the upper and lower fluids have the same velocity, and the upper layer is colder than the lower layer as illustrated in Fig. 1. The mean vertical and horizontal velocities are zero in a Galilean frame moving with the mean velocity and, consequently, convective terms in the k, ϵ, and T transport equations are zero. The governing Eqs. (4), (6), and (7) reduce to:

$$\frac{\partial T}{\partial t} = \frac{\partial}{\partial y}\left(\frac{\nu_t}{\sigma_T}\frac{\partial T}{\partial y}\right) \tag{10}$$

$$\frac{\partial k}{\partial t} = \frac{\partial}{\partial y}\left(\frac{\nu_t}{\sigma_k}\frac{\partial k}{\partial y}\right) + G_b - \epsilon \tag{11}$$

$$\frac{\partial \epsilon}{\partial t} = \frac{\partial}{\partial y}\left(\frac{\nu_t}{\sigma_\epsilon}\frac{\partial \epsilon}{\partial y}\right) + C_{\epsilon 3}\frac{\epsilon}{k}G_b - C_{\epsilon 2}\frac{\epsilon^2}{k} \tag{12}$$

The energy equation is recast in terms of density using a constant expansion coefficient, β.

$$\frac{\partial \rho}{\partial t} = \frac{\partial}{\partial y}\left(\frac{\nu_t}{\sigma_T}\frac{\partial \rho}{\partial y}\right) \tag{13}$$

Initial conditions are:

$$\begin{aligned} &\text{at} \quad t = 0 \quad \text{for} \quad y \geq 0: \quad \rho = \rho_2, \quad k = 0, \quad \epsilon = 0 \\ &\text{at} \quad t = 0 \quad \text{for} \quad y < 0: \quad \rho = \rho_1, \quad k = 0, \quad \epsilon = 0 \end{aligned} \tag{14}$$

Exterior quiescent fluid boundary conditions are applied at the mixing layer boundary, $\pm h(t)$ shown in Fig. 1, as follows:

$$\begin{aligned} &\text{for} \quad y > h: \quad \rho = \rho_2, \quad k = 0, \quad \epsilon = 0 \\ &\text{for} \quad y < -h: \quad \rho = \rho_1, \quad k = 0, \quad \epsilon = 0 \end{aligned} \tag{15}$$

The above set of equations has a self similar solution using the similarity variables: $\eta = y/t^2$, $k(t, y) = t^2\tilde{k}(\eta)$, $\epsilon(t, y) = t\tilde{\epsilon}(\eta)$, $\rho(t, y) = \tilde{\rho}(\eta)$.

Introducing similarity variables into Eqs. (10) to (12) gives the following ordinary differential equations in $\tilde{k}$, $\tilde{\epsilon}$, and $\tilde{\rho}$:

$$-2\eta\frac{d\tilde{\rho}}{d\eta} = \frac{C_\mu}{\sigma_T}\frac{d}{d\eta}\left(\frac{\tilde{k}^2}{\tilde{\epsilon}}\frac{d\tilde{\rho}}{d\eta}\right) \tag{16}$$

$$2\tilde{k} - 2\eta\frac{d\tilde{k}}{d\eta} = \frac{C_\mu}{\sigma_k}\frac{d}{d\eta}\left(\frac{\tilde{k}^2}{\tilde{\epsilon}}\frac{d\tilde{k}}{d\eta}\right) + \frac{C_\mu}{\sigma_T}\frac{\tilde{k}^2}{\tilde{\epsilon}}\frac{g}{\rho_o}\frac{d\tilde{\rho}}{d\eta} - \tilde{\epsilon} \tag{17}$$

$$\tilde{\epsilon} - 2\eta\frac{d\tilde{\epsilon}}{d\eta} = \frac{C_\mu}{\sigma_\epsilon}\frac{d}{d\eta}\left(\frac{\tilde{k}^2}{\tilde{\epsilon}}\frac{d\tilde{\epsilon}}{d\eta}\right) + C_{\epsilon 3}\tilde{k}\frac{g}{\rho_o}\frac{d\tilde{\rho}}{d\eta} - C_{\epsilon 2}\frac{\tilde{\epsilon}^2}{\tilde{k}} \tag{18}$$

The constant $C_{\epsilon 3}$ is calculated from the integration of Eqs. (16) to (18) using approximate profiles for k, ϵ, and ρ. The turbulent kinetic energy and dissipation are approximated by parabolic profiles and the density within the mixing layer is approximated by a linear profile. It is shown later that these profiles are reasonable approximations to the true profiles. The approximate profiles are:

$$\tilde{k} = C_k(1 - \tilde{\eta}^2) \quad \tilde{\epsilon} = C_\epsilon(1 - \tilde{\eta}^2) \quad \tilde{\rho} = C_\rho\tilde{\eta} + \tilde{\rho}_1$$

where the self-similar length scale is normalized based on the mixing half width, $C_w = h/t^2$:

$$\tilde{\eta} = \frac{\eta}{C_w} = \frac{y}{h} \tag{19}$$

C_K and C_ϵ are constants, and for the linear density profile $C_\rho = (\rho_2 - \rho_1)/2$ and $\tilde{\rho}_1 = (\rho_1 + \rho_2)/2$. The equations are integrated across the mixing layer from $-1 < \tilde{\eta} < 1$, and the constants calculated:

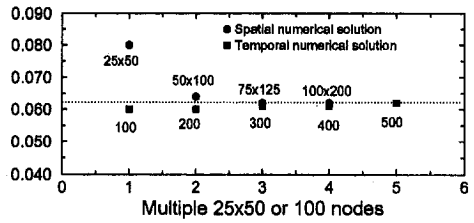

Fig. 2 Grid independence checks for spatial and temporal computed solutions

$$C_k = \frac{B^2 C_\rho^2 (C_{\epsilon 2} - C_{\epsilon 3})^3}{(4C_{\epsilon 2} - 3)^2 (4C_{\epsilon 3} - 3)} \frac{\sigma_T}{C_\mu} \quad C_\epsilon = \frac{(4C_{\epsilon 3} - 3)}{(C_{\epsilon 2} - C_{\epsilon 3})} C_k$$

$$B = -\frac{C_\mu g}{\sigma_T \rho_o} \quad C_W = \frac{C_\mu (4C_{\epsilon 2} - 3)}{B C_\rho \sigma_T (C_{\epsilon 2} - C_{\epsilon 3})} C_k \qquad (20)$$

$C_{\epsilon 2}$, C_μ, and σ_T, in Eqs. (20), are the standard k-ϵ constants, C_ρ is given by the density differences between the layers, and the self-similar mixing width $C_W = h/t^2$ can be obtained from experimental data for the half-width of the mixing layer:

$$h = \alpha \mathrm{A} g t^2 \qquad (21)$$

where A is the Atwood number and α is the growth rate constant of $\alpha = 0.07$ from Snider and Andrews (1994). Solving the C_W Eq. (30) for $C_{\epsilon 3}$ gives a value of $C_{\epsilon 3} = 0.88$.

Numerical One-Dimensional Transient Solution. The transient one-dimensional Eqs. (10) to (12) were solved numerically using a range of $C_{\epsilon 3}$ values around the analytical self-similar value of 0.88. The numerical method used finite volumes, with staggered momentum nodes and a SIMPLE solution method (Patankar, 1980). Transient solutions were made using time steps from 0.05 s to 0.1 s and spatial grids ranging from 100 to 500 nodes uniformly spaced over a computational length of 0.5 m. The total volume error at each time step was less than 10^{-7} m^3. Solutions were found grid independent at nodalizations greater than 200 nodes as shown in Fig. 2.

Two methods can start the transient problem. In the first, the self-similar distribution of k, ϵ, and T are specified across the initial mixing width and the numerical solution quickly becomes self similar. In the second, which is used in this study, reasonable initial values for k, ϵ, and T are specified in an initial mixing width, and the numeric solution, like the experiment, progresses to a self-similar state. In the second approach, a virtual origin is defined which accounts for the development time to self-similar mixing. Both methods produced the same self-similar solution.

Figure 3 shows the growth rate constant, α, for the numerically calculated mixing layer plotted versus $C_{\epsilon 3}$. The $C_{\epsilon 3}$ from the self-similar solution is shown for comparison. The computed $C_{\epsilon 3}$ ranges from 0.88 to 0.94 for the corresponding range of measured growth constants of $\alpha = 0.05$ to 0.077 reported in the literature by Read (1984), Youngs (1992), Linden et al. (1992), Andrews and Spalding (1990), and Snider and Andrews (1994). Figure 3 shows the value $C_{\epsilon 3} = 0.8$ given by Hanjalic and Vasic (1993) gives a mixing layer growth rate $\alpha \sim 0.12$ which is larger than that measured. A value of $C_{\epsilon 3} = 0.91$ gives an $\alpha = 0.07$ which compares well with measurements by Snider and Andrews (1994) and so is used in this study. The computed self-similar k, ϵ, and T compare reasonably with the approximate profiles used in the analytical self-similar solution, which explains the good agreement between analytical and computed $C_{\epsilon 3}$.

Two-Dimensional Steady Boundary Conditions

A two-dimensional plane mixing layer generally forms as two parallel streams at different velocities and different temperatures meet downstream from the splitter plate as illustrated in Fig. 1. The temperature of the bottom stream is higher than that of the top stream giving buoyancy unstable flow. With the same bottom and top velocities, the mixing is from buoyancy only, and with a uniform temperature field, the mixing is from shear only.

Constant freestream velocities U_1 and U_2 and temperatures T_1 and T_2 are applied at the inlet and in the far-field above and below the mixing region. The inlet k was set at 5 percent of the average free stream flow value based on measured data by Browand and Weidman (1976), which had experimental conditions close to those of this study. The inlet dissipation is based on a length scale associated with the 7 mesh/cm screen at the end of the splitter plate and is, $\epsilon_{\text{inlet}} = (k_{\text{inlet}}^{3/2}/l)$, where the length scale is taken as the mesh spacing $l = 0.12$ cm. The gradient of k and ϵ are zero in the far field above and below the mixing layer. The exit boundary condition is local one-way which gives an outflow with no exit streamwise diffusion. The outlet condition matches the parabolic design of the experiment (Snider and Andrews, 1994).

The calculation domain begins near the end of the splitter plate. Flow from the end of the splitter plate forms a wake that is complicated as boundary layers pass through a full screen. The k-ϵ model cannot be expected to work well in the near wake of the splitter plate because of the large change in anisotropy of the Reynolds stresses that occur as flow leaves the solid plate to a free density interface. This study focuses on calculating the developed turbulent mixing layer and requires only reasonable inlet values for the inlet mixing region. The experiment by Snider and Andrews (1994) used a full screen at the end of the splitter plate. Koop (1976) found that the full screen reduced boundary layer effects and gave nearly a step profile across the mixing layer. To model the experiment, the inlet velocity and temperature were specified as error functions across a narrow inlet mixing width. As detailed above the inlet value for k was taken from experimental data by Browand and Weidman (1976) and approximated by a bell shaped curve with a reasonable peak k value of 5 percent of the freestream flow. The initial mixing width was 2 to 3 computational nodes wide, which gave only a sparse representation of the curves. However, our interest was in the fully developed region downstream where profiles develop across many nodes.

Table 1 shows further details of the computations. The calculations are for buoyancy, shear, and compound shear and buoyancy mixing. Two-dimensional steady solutions are listed as "spatial" and the one-dimensional transient calculation is listed as "temporal."

The numerical method used two-dimensional, finite volumes with staggered momentum nodes. A hybrid numerical scheme (Spalding, 1972), and a SIMPLE solution scheme (Patankar, 1980) were employed. Steady calculations were made using node sizes ranging from 25 × 50 to 100 × 200 (axial-streamwise direction by vertical direction). The computation domain was 0.7 m in the streamwise direction and 1.2 m in the vertical

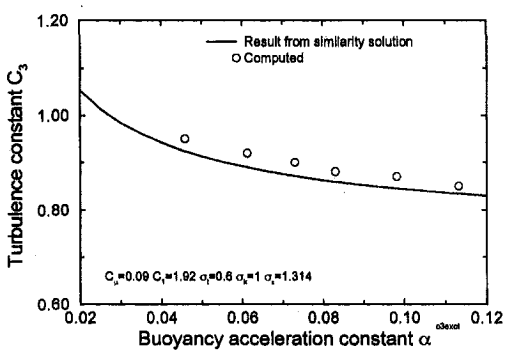

Fig. 3 Turbulence constant $C_{\epsilon 3}$ compared to buoyancy growth constant α

Table 1 Boundary conditions and nodalization for numeric calculations. buoy: buoyancy calculation. shear: shear calculation. spatial: two-dimensional steady calculation. temporal 1-D: one-dimension transient solution.

Run	Exper[1].	Comment	U_1 (cm/s)	U_2 (cm/s)	T_1 (K)	T_2 (K)	Inlet h (cm)	Grid $X \times Y$
1		shear, spatial	3.4	5.4	300.0	300	0.90	50 × 100
2		shear, spatial	5.0	10.0	300.0	300	0.81	50 × 100
3		shear, spatial	4.1	4.7	300.0	300	0.72	50 × 100
4	2–68	buoy, temporal, 1-D	—	—	310.3	306.7	0.19	1 × 500
5	2–68	buoy, spatial	4.8	4.9	310.3	306.7	0.49	50 × 100
6	3–11	buoy and shear, spatial	4.1	4.7	311.2	306.8	0.67	50 × 100
7		buoy, spatial	4.4	4.4	311.2	306.8	0.54	50 × 100
8		buoy and shear, spatial	5.4	3.4	311.2	306.8	0.27	50 × 100

[1] Experiments listed are from Snider and Andrews (1994).

direction. Grid spacing was uniform in the streamwise direction and varied non-linearly in the vertical direction with the vertical grid size on the order of 0.24 cm at the slip line and 8 cm at the far field boundary. The total volume error for convergence was less than 10^{-7} m^3. Solutions were grid independent at node sizes greater than 50 × 100 as shown in Fig. 2. Applying variations in the specified inlet and initial mixing layer widths gave some change in distance (or time) to reach self-similar mixing but did not alter the developed mixing layer growth rate.

Buoyancy Mixing

Our work described above with a one-dimensional mixing model provided a value for $C_{\epsilon 3}$. This section gives results from two-dimensional steady calculations of the buoyancy mixing layer compared with measured data. The two-dimensional solution is motivated by a possible asymmetric behavior produced by shear. A transient analytical approximation of the free shear layer can be made for discontinuous flow (see Schlichting, 1958), but the common self-similar approach uses the two-dimensional boundary layer equations. The two-dimensional equations predict an asymmetric mixing layer that compares well with measured data with the asymmetry vanishing as the free stream velocity ratio exceeds 85 percent (Rajaratnam, 1976). Strong asymmetric mixing layers were not observed nor expected for the experiments predicted in this study, but to ensure that we fully capture the physical processes in both shear mixing, and compound shear and buoyancy mixing the full two-dimensional equations were solved.

Calculated and measured mixing half-widths, h, for a buoyancy layer are compared in Fig. 4. Snider and Andrews (1994) designed the experiment stream velocities to give a parabolic flow where the buoyancy mixing was carried in a moving frame of reference. The upper stream is cooler than the lower stream which gives a buoyancy unstable interface. Experimental results are formed from ensemble averaging a set of measurements. Further, Snider and Andrews (1994) showed that by nondimensioning experimental data, the data collapsed to a single curve in the developed mixing region. Calculated and measured results are presented for only two experiments in this study, but calculations for other tests compare equally well. Results from the spatial two-dimensional calculation (Run 5) and temporal calculation (Run 4) are compared with measured data from Test 2-68 in Fig. 4. There is a central region marked on the figure where the mixing is self-similar and the experimental and numerical results are comparable. Upstream the mixing is developing, and downstream of the marked self-similar region the channel ceiling and floor influence the mixing layer. The measured and calculated data are adjusted to a virtual origin to account for developing flow. Figure 4 shows growth rate differences between the spatial and temporal solutions at the start of the mixing layer. The difference arises from different temporal initial conditions and spatial inlet conditions. For established mixing ($x/W > 3$), the temporal and spatial calculations give the same mixture growth rate independent of inlet or initial conditions, and both calculations compare well with measured data.

Shear Mixing Alone

A two-dimensional, steady calculation of the shear mixing layer with no temperature gradient was made. Table 1 gives the flow conditions for the three shear calculations, Run 1, Run 2, and Run 3. The width of the mixing layer is defined by the vorticity thickness $\delta_\omega = (U_1 - U_2)/(\partial u/\partial y)_{\max}$. As expected for the shear layer, the calculated δ_ω grows linearly with streamwise distance except near the splitter plate. The slope of the calculated vorticity thickness is compared with measured data in Fig. 5. There is a significant spread in the measured data. However, it is evident that the calculated mixing layer thickness compares well and lies within the measured range.

Compound Buoyancy and Shear Mixing

In compound mixing both a temperature and velocity difference are applied between the upper and lower streams. The upper stream is cooler giving a buoyancy unstable interface. The governing equations are solved with turbulence constants defined from canonical shear and buoyancy mixing. Figure 6 compares measured data from Test 3-11 with the predicted mixing layer growth rate from compound shear and buoyancy calculation and from a buoyancy only calculation. Table 1 gives conditions for experimental Test 3-11. Again Test 3-11 is a typical compound mixing experiment where presented data are from ensemble averaging of measured data over the duration of the test. Both calculated and measured data are adjusted to a virtual origin. The steady compound mixing calculation and the pure buoyancy transient calculation agree well with measured data. Considering the good agreement with the pure buoyancy calculation, buoyancy appears as the dominate mixing process for the low shear values of Test 3-11 (ΔU = 0.6 cm/

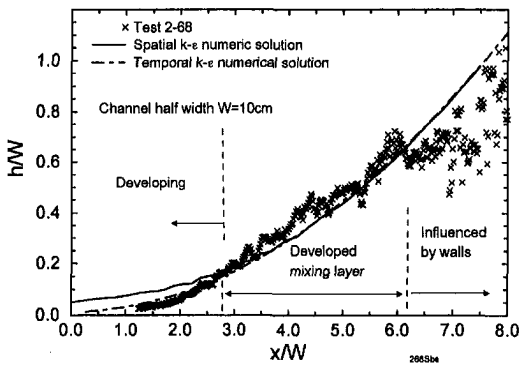

Fig. 4 Calculated pure buoyancy mixing width compared with measured data

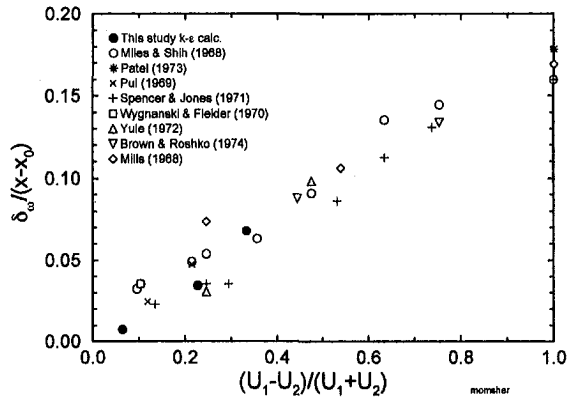

Fig. 5 Shear layer thickness

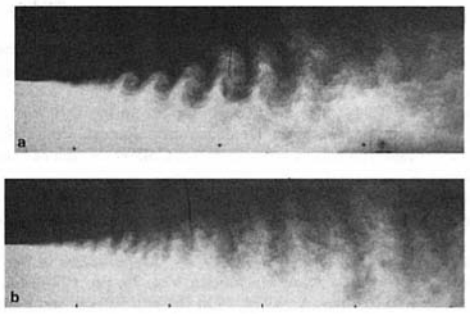

Fig. 7 (*a*) Compound mixing: Test 3-09, U_t = 5.2 cm/s, U_b = 4.3 cm/s Atwood No. = 0.00074, (*b*) Pure buoyancy mixing: Test 2-68, U_t = 4.9 cm/s, U_b = 4.8 cm/s, Atwood No. = 0.00064.

s), as might be expected from its quadratic growth. Figure 6 shows that buoyancy alone has a slightly greater mixing layer growth than for compound shear and buoyancy. We initially thought that the addition of shear to buoyancy mixing might increase the mixing width. However, the figure shows that addition of shear reduced the mixing width. Uncertainty in the experimental measured mixing width at low velocity differences was too large to verify the numerically observed effect of a reduced mixing layer from shear. However, it is important to note that the compound mixing in the experiment did not increase the mixing width, which is in agreement with the calculation.

The nonmechanistic k-ϵ model which balances energy generation and dissipation using constants from canonical shear and buoyancy studies predicts the suppression of the compound unstable shear and buoyancy mixing width. Indeed, numerical calculations beyond the limits of the experiments, with the same mean velocity but high shear rates, predict significant reduction in the mixing width from that of pure buoyancy. The k-ϵ terms represent a competition between the canonical shear and buoyancy mixing, and the ratio of buoyancy to shear turbulence production (Richardson number, $\mathrm{Ri} = -(g(\partial\rho/\partial y)/\rho(\partial u/\partial y)^2)$) near -1 suggests significant contribution by both mechanisms.

To understand better why compound shear and buoyancy do not produce a wider mixing region, we present two photographs in Figs. 7(*a*) and 7(*b*) for measured pure buoyancy mixing and compound mixing. Inspection of the photographs reveals that the cause of the reduced mixing width may be explained mechanistically as skewing and rounding of the normally vertical plumes by the velocity gradient. In a constant convective flow, buoyant plumes are fed from upper and lower streams at the same horizontal velocity and form vertical structures in a moving frame of reference as seen experimentally in Fig. 7(*b*) and illustrated on the left side of Fig. 8. Compound mixing of buoyancy with different stream velocities is seen experimentally in Fig. 7(*a*) and illustrated on the right side in Fig. 8. The buoyant heavy and light fluids interpenetrate each other at near the same rate as that in a constant moving frame of reference. However, the vertical velocity gradient stretches and thins the normally vertical plumes which in turn reduces the vertical height of the structures and the mixing width. Figure 8 illustrates the process where fast, heavy fluid (white) enters the mixing layer from the upper side, and slow, light fluid (gray) enters the mixing layer from the lower side. The high velocity stream entering the top of mixing layer pushes rising plumes of originally slow fluid, and the lower, slow stream drags descending plumes of originally fast fluid. This skews plumes and forms vortices that appear similar to shear layer mixing. The result of compound mixing is stretched, skewed plumes with rounded fronts and a reduced mixing growth rate.

Concluding Remarks

The k-ϵ model predicted well the pure buoyancy mixing layer and the compound shear and buoyancy mixing layer. A transient one-dimensional solution or a two-dimensional steady solution did equally well in predicting the pure buoyancy mixing layer. The turbulence constant $C_{\epsilon 3} = 0.91$ defined here for a buoyancy mixing layer provides good predictions for all cases.

Adding shear to an unstable buoyancy mixing layer does not increase the mixing growth rate beyond that from buoyancy alone. The measured flow structures suggest that shear skewing and stretching of vertical buoyant plumes reduces the growth of a unstable buoyancy mixing layer. The velocity difference in the available experimental data was too low to quantify differences in growth rate for buoyancy mixing width with and without shear. Further experiments with higher shear rates are required to resolve the differences.

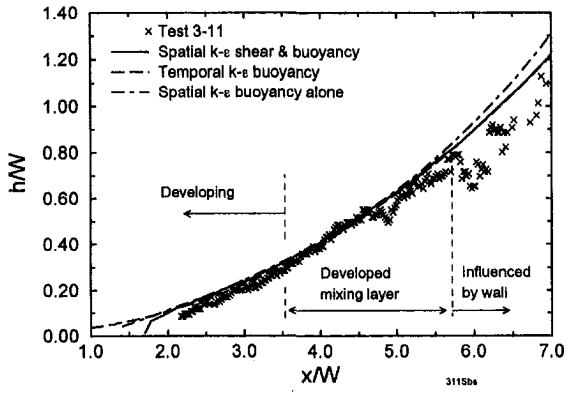

Fig. 6 Calculated combined shear and buoyancy mixing width compared with measured data

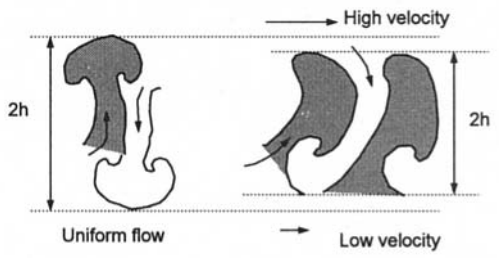

Fig. 8 Illustration of the buoyancy mixing and combined shear and buoyancy

References

Andrews, M. J., and Spalding, D. B., 1990, "A Simple Experiment to Investigate Two-Dimensional Mixing by Rayleigh-Taylor Instability," *Physics of Fluids,* Vol. 2, pp. 922–927.

Andrews, M. J., 1984, "The k-ϵ Model Applied to the Development of Rayleigh-Taylor Instability," Phoenix Demonstration Report, PDR/CFDU IC/13, Computational Fluid Mechanics Unit, Imperial College of Science and Technology, London, UK.

Bradshaw, P., Launder, B. E., and Lumley, J., 1991, "Collaborative Testing of Turbulence Models," ASME JOURNAL OF FLUIDS ENGINEERING, Vol. 113, pp. 3–4.

Browand, F. K., and Weidman, P. D., 1976, "Large Scales in the Developing Mixing Layer," *Journal of Fluid Mechanics,* Vol. 76, pp. 127–144.

Brown, G. L., and Roshko, A., 1974, "On Density Effects and Large Structure in Turbulent Mixing Layers," *Journal of Fluid Mechanics,* Vol. 64, pp. 775–816.

Chandrasekhar, S., 1961, *Hydrodynamic and Hydromagnetic Stability,* Oxford University Press.

Comte, P., Lesieur, M., Laroche, H., and Normand, X., 1989, "Numerical Simulation of Turbulent Plane Shear Layers," *Turbulent Shear Flow 6,* Springer-Verlag, Berlin, pp. 360–380.

Deardorff, J. W., 1970, "Convective Velocity and Temperature Scale for the Unstable Planetary Boundary Layer and for Rayleigh Convection," *Journal of Atmospheric Sciences,* Vol. 27, pp. 1211–1213.

Dhir, V. K., and Chang, F., 1992, "Heat Transfer Enhancement Using Tangential Injection," *ASHRAE Transactions,* BA-92-4-1.

Hanjalic, K., and Vasic, S., 1993, "Some Further Exploration of Turbulence Models for Buoyancy Driven Flows," *Turbulent Shear Flow 8,* Springer-Verlag, Berlin, pp. 319–341.

Hanjalic, K., 1994, "Achievements and Limitations in Modeling and Computation of Buoyant Turbulent Flows and Heat Transfer," *Proceedings Tenth International Heat Transfer Conference,* Brighton, UK, Vol. 1, Taylor Francis Publishing Co., pp. 1–18.

Imberger, J., and Hamblin, P. F., 1982, "Dynamics of Lakes and Cooling Ponds," *Annual Review of Fluid Mechanics,* pp. 153–187.

Koop, G. K., 1976, "Instability and Turbulence in a Stratified Shear Layer," Ph.D. thesis, University of Southern California.

Launder, B. E., Morse, A. P., Rodi, W., and Spalding, D. B., 1973, "The Prediction of Free-Stream Flows—A Comparison of the Performance of Six Turbulence Models," NASA *SP* 320.

Launder, B. E., 1988, "On the Computation of Convective Heat Transfer in Complex Turbulent Flows," ASME *Journal of Heat Transfer,* Vol. 110, pp. 1112–1128.

Launder, B. E., and Spalding, D. B., 1974, "The Numerical Computation of Turbulent Flows," *Computer Methods in Applied Mechanics and Engineering,* pp. 269–289.

Li, X. L., 1993, "Study of Three Dimensional Rayleigh Taylor Instabilities in Compressible Fluids Through Level Set Method and Parallel Computation," *Physics of Fluids A,* Vol. 5, pp. 1904–1913.

Linden, P. F., Redondo, J. M., and Caulfield, C. P., 1992, "Molecular Mixing in Rayleigh-Taylor Instability," *Advances in Compressible Turbulent Mixing,* W. P. Dannevik, A. C. Buckingham, and C. E. Leith, eds., pp. 95–104.

Miles, J. B., and Shih, J., 1968, "Similarity Parameter for Two-Stream Turbulent Jet-Mixing Region," *Journal AIAA,* Vol. 6, p. 1429.

Mills, R. D., 1968, "Numerical and Experimental Investigation of the Shear Layer Between Two Parallel Streams," *Journal of Fluid Mechanics,* Vol. 33, p. 591.

Patankar, S. V., 1980, *Numerical Heat Transfer and Fluid Flow,* Hemisphere Publishing Co.

Patel, R. P., 1973, "An Experimental Study of a Plane Mixing Layer," *Journal AIAA,* Vol. 11, p. 67.

Pui, N. K., 1969, "The Plane Mixing Layer Between Parallel Streams," M.A. Science thesis, University of British Columbia.

Rajaratnam, N., 1976, *Turbulent Jets,* Elsevier Science Publishing, Amsterdam, pp. 87–114.

Read, K. I., "Experimental Investigation of Turbulent Mixing by Rayleigh-Taylor Instability," *Physica 12D,* pp. 45–58, 1984.

Rodi, W., 1993, *Turbulence Models and Their Application in Hydraulics, A State of the Art Review,* Third edition, AA Balkema, Rotterdam, Brookfield.

Rodi, W., 1991, "Examples of Turbulence Model Applications," *Introduction to the Modeling of Turbulence,* vonKarmen Institute for Fluid Dynamics, Lecture Series 1991-02.

Rogers, M. M., and Moser, R. D., 1994, "Direct Simulation of a Self-Similar Turbulent Mixing Layer," *Physics of Fluids,* Vol. 6, pp. 903–923.

Sharp, D. H., 1984, "An Overview of Rayleigh-Taylor Instability," *Physica 12D,* p. 3.

Schlichting, H., 1958, *Boundary Layer Theory,* McGraw-Hill, NY, p. 489.

Spalding, D. B., 1972, "A Novel Finite-Difference Formulation for Differential Expressions Involving Both First and Second Derivatives," *International Journal for Numerical Methods Engineering,* Vol. 4, p. 551.

Spencer, B. W., and Jones, B. G., 1971, "Statistical Investigation of Pressure and Velocity Fields in the Turbulent Two-Stream Mixing Layer," *AIAA Paper* no. 71-613.

Spitz, P. B., and Haas, J., 1991, "Numerical Calibration of Rayleigh-Taylor Induced Turbulent Flows With k-ϵ Mix Model," *Proceedings of the 3rd International Workshop on the Physics of Compressible Turbulent Mixing,* Royaumont, pp. 511–521.

Snider, D. M., and Andrews, M. J., 1994a, "Rayleigh-Taylor and Shear Driven Mixing with an Unstable Thermal Stratification," *Boundary Layer and Free Shear Flows,* J. F. Donovan and J. C. Dutton, eds., ASME Fluids Summer Meeting 1994.

Taylor, G. I., 1950, "The Instability of Liquid Surfaces When Accelerated in a Direction Perpendicular to Their Planes I," *Proceedings of the Royal Society of London Series A,* Vol. CCI, pp. 192–196.

Tennekes, H., and Lumley, J. L., 1972, *A First Course in Turbulence,* MIT Press, pp. 97–102.

Vinnichenko, N. K., Pinus, N. Z., Shmeter, S. M., and Shur, G. N., 1980, *Turbulence in the Free Atmosphere,* Consultants Bureau, NY, pp. 145–164.

White, F. M., 1991, *Viscous Fluid Flow,* McGraw-Hill, Inc., pp. 482–483.

Wygnanski, I., and Fielder, H. E., 1970, "The Two-Dimensional Mixing Region," *Journal of Fluid Mechanics,* Vol. 41, p. 327.

Yang, R. J., and Aung, W., 1985, "Equations and Coefficients for Turbulence Modeling," *Natural Convection Fundamentals and Applications,* Hemisphere Publishing Co.

Yule, A. J., 1972, "Two-Dimensional Self-Preserving Turbulent Mixing Layers at Different Free Stream Velocity Ratios," *Aero. Res. Counc. R&M.,* no. 3683.

Youngs, D. L., 1991, "Three-Dimensional Numerical Simulation of Turbulent Mixing by Rayleigh-Taylor Instability," *Physics of Fluids A,* pp. 1312–1320.

Youngs, D. L., 1992, "Numerical Simulation of Turbulent Mixing by Experimental Investigation of Turbulent Mixing by Rayleigh-Taylor Instability," *Advances in Compressible Turbulent Mixing,* W. P. Dannevik, A. C. Buckingham, and C. E. Leith, eds., pp. 607–626.

Youngs, D. L., 1984, "Numerical Simulation of Turbulent Mixing by Rayleigh-Taylor Instability," *Physica 12D,* pp. 32–44.